

Evidence for $e^+e^- \rightarrow \eta_c(1S)$ at center-of-mass energies between 4.01 and 4.60 GeV

M. Ablikim,¹ M. N. Achasov,^{9,d} S. Ahmed,¹⁴ M. Albrecht,⁴ M. Alekseev,^{53a,53c} A. Amoroso,^{53a,53c} F. F. An,¹ Q. An,^{50,40} J. Z. Bai,¹ Y. Bai,³⁹ O. Bakina,²⁴ R. Baldini Ferroli,^{20a} Y. Ban,³² D. W. Bennett,¹⁹ J. V. Bennett,⁵ N. Berger,²³ M. Bertani,^{20a} D. Bettoni,^{21a} J. M. Bian,⁴⁷ F. Bianchi,^{53a,53c} E. Boger,^{24,b} I. Boyko,²⁴ R. A. Briere,⁵ H. Cai,⁵⁵ X. Cai,^{1,40} O. Cakir,^{43a} A. Calcaterra,^{20a} G. F. Cao,^{1,44} S. A. Cetin,^{43b} J. Chai,^{53c} J. F. Chang,^{1,40} G. Chelkov,^{24,b,c} G. Chen,¹ H. S. Chen,^{1,44} J. C. Chen,¹ M. L. Chen,^{1,40} S. J. Chen,³⁰ X. R. Chen,²⁷ Y. B. Chen,^{1,40} X. K. Chu,³² G. Cibinetto,^{21a} H. L. Dai,^{1,40} J. P. Dai,^{35,h} A. Dbeyssi,¹⁴ D. Dedovich,²⁴ Z. Y. Deng,¹ A. Denig,²³ I. Denysenko,²⁴ M. Destefanis,^{53a,53c} F. De Mori,^{53a,53c} Y. Ding,²⁸ C. Dong,³¹ J. Dong,^{1,40} L. Y. Dong,^{1,44} M. Y. Dong,^{1,40,44} O. Dorjkhaidav,²² Z. L. Dou,³⁰ S. X. Du,⁵⁷ P. F. Duan,¹ J. Fang,^{1,40} S. S. Fang,^{1,44} X. Fang,^{50,40} Y. Fang,¹ R. Farinelli,^{21a,21b} L. Fava,^{53b,53c} S. Fegan,²³ F. Feldbauer,²³ G. Felici,^{20a} C. Q. Feng,^{50,40} E. Fioravanti,^{21a} M. Fritsch,^{23,14} C. D. Fu,¹ Q. Gao,¹ X. L. Gao,^{50,40} Y. Gao,⁴² Y. G. Gao,⁶ Z. Gao,^{50,40} B. Garillon,²³ I. Garzia,^{21a} K. Goetzen,¹⁰ L. Gong,³¹ W. X. Gong,^{1,40} W. Gradl,²³ M. Greco,^{53a,53c} M. H. Gu,^{1,40} S. Gu,¹⁵ Y. T. Gu,¹² A. Q. Guo,¹ L. B. Guo,²⁹ R. P. Guo,¹ Y. P. Guo,²³ Z. Haddadi,²⁶ S. Han,⁵⁵ X. Q. Hao,¹⁵ F. A. Harris,⁴⁵ K. L. He,^{1,44} X. Q. He,⁴⁹ F. H. Heinsius,⁴ T. Held,⁴ Y. K. Heng,^{1,40,44} T. Holtmann,⁴ Z. L. Hou,¹ C. Hu,²⁹ H. M. Hu,^{1,44} T. Hu,^{1,40,44} Y. Hu,¹ G. S. Huang,^{50,40} J. S. Huang,¹⁵ S. H. Huang,⁴¹ X. T. Huang,³⁴ X. Z. Huang,³⁰ Z. L. Huang,²⁸ T. Hussain,⁵² W. Ikegami Andersson,⁵⁴ Q. Ji,¹ Q. P. Ji,¹⁵ X. B. Ji,^{1,44} X. L. Ji,^{1,40} X. S. Jiang,^{1,40,44} X. Y. Jiang,³¹ J. B. Jiao,³⁴ Z. Jiao,¹⁷ D. P. Jin,^{1,40,44} S. Jin,^{1,44} Y. Jin,⁴⁶ T. Johansson,⁵⁴ A. Julin,⁴⁷ N. Kalantar-Nayestanaki,²⁶ X. L. Kang,¹ X. S. Kang,³¹ M. Kavatsyuk,²⁶ B. C. Ke,⁵ T. Khan,^{50,40} A. Khokkaz,⁴⁸ P. Kiese,²³ R. Kliemt,¹⁰ L. Koch,¹⁰ O. B. Kolcu,^{43b,f} B. Kopf,⁴ M. Kornicer,⁴⁵ M. Kuemmel,⁴ M. Kuhlmann,⁴ A. Kupsc,⁵⁴ W. Kühn,²⁵ J. S. Lange,²⁵ M. Lara,¹⁹ P. Larin,¹⁴ L. Lavezzi,^{53c} H. Leithoff,²³ C. Leng,^{53c} C. Li,⁵⁴ Cheng Li,^{50,40} D. M. Li,⁵⁷ F. Li,^{1,40} F. Y. Li,³² G. Li,¹ H. B. Li,^{1,44} H. J. Li,¹ J. C. Li,¹ Jin Li,³³ K. Li,³⁴ K. Li,¹³ K. J. Li,⁴¹ Lei Li,³ P. L. Li,^{50,40} P. R. Li,^{44,7} Q. Y. Li,³⁴ T. Li,³⁴ W. D. Li,^{1,44} W. G. Li,¹ X. L. Li,³⁴ X. N. Li,^{1,40} X. Q. Li,³¹ Z. B. Li,⁴¹ H. Liang,^{50,40} Y. F. Liang,³⁷ Y. T. Liang,²⁵ G. R. Liao,¹¹ D. X. Lin,¹⁴ B. Liu,^{35,h} B. J. Liu,¹ C. X. Liu,¹ D. Liu,^{50,40} F. H. Liu,³⁶ Fang Liu,¹ Feng Liu,⁶ H. B. Liu,¹² H. H. Liu,¹⁶ H. H. Liu,¹⁶ H. M. Liu,^{1,44} J. B. Liu,^{50,40} J. Y. Liu,¹ K. Liu,⁴² K. Y. Liu,²⁸ Ke Liu,⁶ L. D. Liu,³² P. L. Liu,^{1,40} Q. Liu,⁴⁴ S. B. Liu,^{50,40} X. Liu,²⁷ Y. B. Liu,³¹ Z. A. Liu,^{1,40,44} Zhiqing Liu,²³ Y. F. Long,³² X. C. Lou,^{1,40,44} H. J. Lu,¹⁷ J. G. Lu,^{1,40} Y. Lu,¹ Y. P. Lu,^{1,40} C. L. Luo,²⁹ M. X. Luo,⁵⁶ X. L. Luo,^{1,40} X. R. Lyu,⁴⁴ F. C. Ma,²⁸ H. L. Ma,¹ L. L. Ma,³⁴ M. M. Ma,¹ Q. M. Ma,¹ T. Ma,¹ X. N. Ma,³¹ X. Y. Ma,^{1,40} Y. M. Ma,³⁴ F. E. Maas,¹⁴ M. Maggiora,^{53a,53c} Q. A. Malik,⁵² Y. J. Mao,³² Z. P. Mao,¹ S. Marcello,^{53a,53c} Z. X. Meng,⁴⁶ J. G. Messchendorp,²⁶ G. Mezzadri,^{21b} J. Min,^{1,40} T. J. Min,¹ R. E. Mitchell,¹⁹ X. H. Mo,^{1,40,44} Y. J. Mo,⁶ C. Morales Morales,¹⁴ G. Morello,^{20a} N. Yu. Muchnoi,^{9,d} H. Muramatsu,⁴⁷ A. Mustafa,⁴ Y. Nefedov,²⁴ F. Nerling,¹⁰ I. B. Nikolaev,^{9,d} Z. Ning,^{1,40} S. Nisar,⁸ S. L. Niu,^{1,40} X. Y. Niu,¹ S. L. Olsen,³³ Q. Ouyang,^{1,40,44} S. Pacetti,^{20b} Y. Pan,^{50,40} M. Papenbrock,⁵⁴ P. Patteri,^{20a} M. Pelizaeus,⁴ J. Pellegrino,^{53a,53c} H. P. Peng,^{50,40} K. Peters,^{10,g} J. Pettersson,⁵⁴ J. L. Ping,²⁹ R. G. Ping,^{1,44} A. Pitka,²³ R. Poling,⁴⁷ V. Prasad,^{50,40} H. R. Qi,² M. Qi,³⁰ T. Y. Qi,² S. Qian,^{1,40} C. F. Qiao,⁴⁴ N. Qin,⁵⁵ X. S. Qin,⁴ Z. H. Qin,^{1,40} J. F. Qiu,¹ K. H. Rashid,^{52,i} C. F. Redmer,²³ M. Richter,⁴ M. Ripka,²³ M. Rolo,^{53c} G. Rong,^{1,44} Ch. Rosner,¹⁴ A. Sarantsev,^{24,e} M. Savrić,^{21b} C. Schnier,⁴ K. Schoenning,⁵⁴ W. Shan,³² M. Shao,^{50,40} C. P. Shen,² P. X. Shen,³¹ X. Y. Shen,^{1,44} H. Y. Sheng,¹ M. R. Shepherd,¹⁹ J. J. Song,³⁴ W. M. Song,³⁴ X. Y. Song,¹ S. Sosio,^{53a,53c} C. Sowa,⁴ S. Spataro,^{53a,53c} G. X. Sun,¹ J. F. Sun,¹⁵ L. Sun,⁵⁵ S. S. Sun,^{1,44} X. H. Sun,¹ Y. J. Sun,^{50,40} Y. K. Sun,^{50,40} Y. Z. Sun,¹ Z. J. Sun,^{1,40} Z. T. Sun,¹⁹ C. J. Tang,³⁷ G. Y. Tang,¹ X. Tang,¹ I. Tapan,^{43c} M. Tiemens,²⁶ B. T. Tsednee,²² I. Uman,^{43d} G. S. Varner,⁴⁵ B. Wang,¹ B. L. Wang,⁴⁴ D. Wang,³² D. Y. Wang,³² Dan Wang,⁴⁴ K. Wang,^{1,40} L. L. Wang,¹ L. S. Wang,¹ M. Wang,³⁴ P. Wang,¹ P. L. Wang,¹ W. P. Wang,^{50,40} X. F. Wang,⁴² Y. Wang,³⁸ Y. D. Wang,¹⁴ Y. F. Wang,^{1,40,44} Y. Q. Wang,²³ Z. Wang,^{1,40} Z. G. Wang,^{1,40} Z. H. Wang,^{50,40} Z. Y. Wang,¹ Z. Y. Wang,¹ T. Weber,²³ D. H. Wei,¹¹ J. H. Wei,³¹ P. Weidenkaff,²³ S. P. Wen,¹ U. Wiedner,⁴ M. Wolke,⁵⁴ L. H. Wu,¹ L. J. Wu,¹ Z. Wu,^{1,40} L. Xia,^{50,40} Y. Xia,¹⁸ D. Xiao,¹ H. Xiao,⁵¹ Y. J. Xiao,¹ Z. J. Xiao,²⁹ X. H. Xie,⁴¹ Y. G. Xie,^{1,40} Y. H. Xie,⁶ X. A. Xiong,¹ Q. L. Xiu,^{1,40} G. F. Xu,¹ J. J. Xu,¹ L. Xu,¹ Q. J. Xu,¹³ Q. N. Xu,⁴⁴ X. P. Xu,³⁸ L. Yan,^{53a,53c} W. B. Yan,^{50,40} W. C. Yan,² Y. H. Yan,¹⁸ H. J. Yang,^{35,h} H. X. Yang,¹ L. Yang,⁵⁵ Y. H. Yang,³⁰ Y. X. Yang,¹¹ M. Ye,^{1,40} M. H. Ye,⁷ J. H. Yin,¹ Z. Y. You,⁴¹ B. X. Yu,^{1,40,44} C. X. Yu,³¹ J. S. Yu,²⁷ C. Z. Yuan,^{1,44} Y. Yuan,¹ A. Yuncu,^{43b,a} A. A. Zafar,⁵² Y. Zeng,¹⁸ Z. Zeng,^{50,40} B. X. Zhang,¹ B. Y. Zhang,^{1,40} C. C. Zhang,¹ D. H. Zhang,¹ H. H. Zhang,⁴¹ H. Y. Zhang,^{1,40} J. Zhang,¹ J. L. Zhang,¹ J. Q. Zhang,¹ J. W. Zhang,^{1,40,44} J. Y. Zhang,¹ J. Z. Zhang,^{1,44} K. Zhang,¹ L. Zhang,⁴² S. Q. Zhang,³¹ X. Y. Zhang,³⁴ Y. Zhang,¹ Y. Zhang,¹ Y. H. Zhang,^{1,40} Y. T. Zhang,^{50,40} Yu Zhang,⁴⁴ Z. H. Zhang,⁶ Z. P. Zhang,⁵⁰ Z. Y. Zhang,⁵⁵ G. Zhao,¹ J. W. Zhao,^{1,40} J. Y. Zhao,¹ J. Z. Zhao,^{1,40} Lei Zhao,^{50,40} Ling Zhao,¹ M. G. Zhao,³¹ Q. Zhao,¹ S. J. Zhao,⁵⁷ T. C. Zhao,¹ Y. B. Zhao,^{1,40} Z. G. Zhao,^{50,40} A. Zhemchugov,^{24,b} B. Zheng,^{51,14} J. P. Zheng,^{1,40} W. J. Zheng,³⁴ Y. H. Zheng,⁴⁴ B. Zhong,²⁹ L. Zhou,^{1,40} X. Zhou,⁵⁵ X. K. Zhou,^{50,40} X. R. Zhou,^{50,40} X. Y. Zhou,¹ J. Zhu,⁴¹ K. Zhu,¹ K. J. Zhu,^{1,40,44} S. Zhu,¹ S. H. Zhu,⁴⁹ X. L. Zhu,⁴² Y. C. Zhu,^{50,40} Y. S. Zhu,^{1,44} Z. A. Zhu,^{1,44} J. Zhuang,^{1,40} B. S. Zou,¹ and J. H. Zou¹

(BESIII Collaboration)

- ¹*Institute of High Energy Physics, Beijing 100049, People's Republic of China*
²*Beihang University, Beijing 100191, People's Republic of China*
³*Beijing Institute of Petrochemical Technology, Beijing 102617, People's Republic of China*
⁴*Bochum Ruhr-University, D-44780 Bochum, Germany*
⁵*Carnegie Mellon University, Pittsburgh, Pennsylvania 15213, USA*
⁶*Central China Normal University, Wuhan 430079, People's Republic of China*
⁷*China Center of Advanced Science and Technology, Beijing 100190, People's Republic of China*
⁸*COMSATS Institute of Information Technology, Lahore, Defence Road, Off Raiwind Road, 54000 Lahore, Pakistan*
⁹*G. I. Budker Institute of Nuclear Physics SB RAS (BINP), Novosibirsk 630090, Russia*
¹⁰*GSI Helmholtzcentre for Heavy Ion Research GmbH, D-64291 Darmstadt, Germany*
¹¹*Guangxi Normal University, Guilin 541004, People's Republic of China*
¹²*Guangxi University, Nanning 530004, People's Republic of China*
¹³*Hangzhou Normal University, Hangzhou 310036, People's Republic of China*
¹⁴*Helmholtz Institute Mainz, Johann-Joachim-Becher-Weg 45, D-55099 Mainz, Germany*
¹⁵*Henan Normal University, Xinxiang 453007, People's Republic of China*
¹⁶*Henan University of Science and Technology, Luoyang 471003, People's Republic of China*
¹⁷*Huangshan College, Huangshan 245000, People's Republic of China*
¹⁸*Hunan University, Changsha 410082, People's Republic of China*
¹⁹*Indiana University, Bloomington, Indiana 47405, USA*
^{20a}*INFN Laboratori Nazionali di Frascati, I-00044 Frascati, Italy*
^{20b}*INFN and University of Perugia, I-06100 Perugia, Italy*
^{21a}*INFN Sezione di Ferrara, I-44122 Ferrara, Italy*
^{21b}*University of Ferrara, I-44122 Ferrara, Italy*
²²*Institute of Physics and Technology, Peace Ave. 54B, Ulaanbaatar 13330, Mongolia*
²³*Johannes Gutenberg University of Mainz, Johann-Joachim-Becher-Weg 45, D-55099 Mainz, Germany*
²⁴*Joint Institute for Nuclear Research, 141980 Dubna, Moscow region, Russia*
²⁵*Justus-Liebig-Universitaet Giessen, II. Physikalisches Institut, Heinrich-Buff-Ring 16, D-35392 Giessen, Germany*
²⁶*KVI-CART, University of Groningen, NL-9747 AA Groningen, The Netherlands*
²⁷*Lanzhou University, Lanzhou 730000, People's Republic of China*
²⁸*Liaoning University, Shenyang 110036, People's Republic of China*
²⁹*Nanjing Normal University, Nanjing 210023, People's Republic of China*
³⁰*Nanjing University, Nanjing 210093, People's Republic of China*
³¹*Nankai University, Tianjin 300071, People's Republic of China*
³²*Peking University, Beijing 100871, People's Republic of China*
³³*Seoul National University, Seoul 151-747 Korea*
³⁴*Shandong University, Jinan 250100, People's Republic of China*
³⁵*Shanghai Jiao Tong University, Shanghai 200240, People's Republic of China*
³⁶*Shanxi University, Taiyuan 030006, People's Republic of China*
³⁷*Sichuan University, Chengdu 610064, People's Republic of China*
³⁸*Soochow University, Suzhou 215006, People's Republic of China*
³⁹*Southeast University, Nanjing 211100, People's Republic of China*
⁴⁰*State Key Laboratory of Particle Detection and Electronics, Beijing 100049, Hefei 230026, People's Republic of China*
⁴¹*Sun Yat-Sen University, Guangzhou 510275, People's Republic of China*
⁴²*Tsinghua University, Beijing 100084, People's Republic of China*
^{43a}*Ankara University, 06100 Tandogan, Ankara, Turkey*
^{43b}*Istanbul Bilgi University, 34060 Eyup, Istanbul, Turkey*
^{43c}*Uludag University, 16059 Bursa, Turkey*
^{43d}*Near East University, Nicosia, North Cyprus, Mersin 10, Turkey*
⁴⁴*University of Chinese Academy of Sciences, Beijing 100049, People's Republic of China*
⁴⁵*University of Hawaii, Honolulu, Hawaii 96822, USA*
⁴⁶*University of Jinan, Jinan 250022, People's Republic of China*
⁴⁷*University of Minnesota, Minneapolis, Minnesota 55455, USA*
⁴⁸*University of Muenster, Wilhelm-Klemm-Str. 9, 48149 Muenster, Germany*
⁴⁹*University of Science and Technology Liaoning, Anshan 114051, People's Republic of China*
⁵⁰*University of Science and Technology of China, Hefei 230026, People's Republic of China*
⁵¹*University of South China, Hengyang 421001, People's Republic of China*
⁵²*University of the Punjab, Lahore 54590, Pakistan*

^{53a}*University of Turin, I-10125 Turin, Italy*^{53b}*University of Eastern Piedmont, I-15121 Alessandria, Italy*^{53c}*INFN, I-10125 Turin, Italy*⁵⁴*Uppsala University, Box 516, SE-75120 Uppsala, Sweden*⁵⁵*Wuhan University, Wuhan 430072, People's Republic of China*⁵⁶*Zhejiang University, Hangzhou 310027, People's Republic of China*⁵⁷*Zhengzhou University, Zhengzhou 450001, People's Republic of China*

(Received 19 May 2017; revised manuscript received 13 July 2017; published 6 September 2017)

We present first evidence for the process $e^+e^- \rightarrow \gamma\eta_c(1S)$ at six center-of-mass energies between 4.01 and 4.60 GeV using data collected by the BESIII experiment operating at BEPCII. We measure the Born cross section at each energy using a combination of twelve $\eta_c(1S)$ decay channels. We also combine all six energies under various assumptions for the energy-dependence of the cross section. If the process is assumed to proceed via the $Y(4260)$, we measure a peak Born cross section $\sigma_{\text{peak}}(e^+e^- \rightarrow \gamma\eta_c(1S)) = 2.11 \pm 0.49(\text{stat.}) \pm 0.36(\text{syst.})$ pb with a statistical significance of 4.2σ .

DOI: 10.1103/PhysRevD.96.051101

The $Y(4260)$, first discovered by *BABAR* in the initial state radiation (ISR) process $e^+e^- \rightarrow \gamma_{\text{ISR}}Y(4260) \rightarrow \gamma_{\text{ISR}}\pi^+\pi^-J/\psi$ [1], cannot be easily explained within the traditional $c\bar{c}$ picture of charmonium. From its production mechanism, we know its spin (J), parity (P), and charge-parity (C) quantum numbers are $J^{PC} = 1^{--}$. However, due to its distinct mass, it cannot be identified with the previously established ψ states in this region [2]. Furthermore, while the $\psi(4040)$, $\psi(4160)$, and $\psi(4415)$ states are thought to be the $n^{2S+1}L_J = 3^3S_1$, 2^3D_1 , and 4^3S_1 states of charmonium, respectively [3], the $Y(4260)$ appears to be supernumerary.

One possibility is that the $Y(4260)$ is a hybrid meson [4,5]. If so, recent lattice QCD calculations predict that its rate of decay to $\gamma\eta_c(1S)$ will be enhanced relative to $\gamma\chi_{c0}(1P)$ [6]. This is in stark contrast to the pattern for conventional ψ states, where, for example, the $\psi(2S)$ decays to $\gamma\chi_{c0}(1P)$ about 30 times more often than to $\gamma\eta_c(1S)$. Finding evidence for $Y(4260) \rightarrow \gamma\eta_c(1S)$ could thus give additional support to the hybrid interpretation.

In this paper, we search for the process $e^+e^- \rightarrow \gamma\eta_c$ (where η_c always denotes $\eta_c(1S)$) using data collected by

the BESIII detector operating at the Beijing Electron Positron Collider (BEPCII). We use a total integrated luminosity of 4.6 fb^{-1} spread among six center-of-mass energies (E_{CM}): 482 pb^{-1} at 4.01 GeV, 1092 pb^{-1} at 4.23 GeV, 826 pb^{-1} at 4.26 GeV, 540 pb^{-1} at 4.36 GeV, 1074 pb^{-1} at 4.42 GeV, and 567 pb^{-1} at 4.60 GeV [7,8].

We first measure the Born cross section at each E_{CM} using the twelve largest decay channels of the η_c : $2(\pi^+\pi^-\pi^0)$, $\pi^+\pi^-\pi^0\pi^0$, $\pi^+\pi^+\pi^-\pi^-\eta$, $K^+K^-\pi^+\pi^-\pi^0$, $2(\pi^+\pi^-)$, $3(\pi^+\pi^-)$, $\pi^+\pi^-\eta$, $K^\pm K_S \pi^\mp \pi^\pm \pi^\mp$, $K^\pm K_S \pi^\mp$, $K^+K^-\pi^0$, $K^+K^-\pi^+\pi^-$, and $K^+K^-\pi^+\pi^-\pi^-$. We then combine the data from the six E_{CM} under four different assumptions about the energy-dependence of the cross section: (1) σ_{FLAT} : the cross section is constant, consistent with the calculation in Ref. [9]; (2) σ_{BELLE} : the cross section follows the Belle parametrization of $\sigma(e^+e^- \rightarrow \pi^+\pi^-J/\psi)$ found in Ref. [10], modeled with a $Y(4008)$ in addition to the $Y(4260)$; (3) $\sigma_{Y(4260)}$: the cross section follows a nonrelativistic Breit-Wigner distribution for the $Y(4260)$ with mass and width values from the Particle Data Group (PDG) [2]; and (4) $\sigma_{Y(4360)}$: the cross section follows a nonrelativistic Breit-Wigner distribution for the $Y(4360)$ with mass and width values from the PDG. Combining the data samples in this way allows us to search for $e^+e^- \rightarrow \gamma\eta_c$ using a larger sample of events and allows us to compare the $Y(4260)$ hypothesis ($\sigma_{Y(4260)}$) to other hypotheses.

The BEPCII e^+e^- storage ring is designed to have a peak luminosity of $10^{33} \text{ cm}^{-2} \text{ s}^{-1}$ at a beam energy of 1.89 GeV [11]. The BESIII detector is a general purpose hadron detector built around the collision point at BEPCII [12]. Charged particles are detected in the main drift chamber (MDC) and are bent by an on-axis 1 Tesla solenoidal magnetic field, yielding a momentum resolution of 0.5% at 1 GeV/ c . Time-of-flight (TOF) scintillation counters are placed around the MDC and provide a timing resolution of 80 ps in the barrel and 110 ps in the end caps. Photons are detected by the electromagnetic calorimeter (EMC)

^aAlso at Bogazici University, 34342 Istanbul, Turkey.^bAlso at the Moscow Institute of Physics and Technology, Moscow 141700, Russia.^cAlso at the Functional Electronics Laboratory, Tomsk State University, Tomsk, 634050, Russia.^dAlso at the Novosibirsk State University, Novosibirsk, 630090, Russia.^eAlso at the NRC ‘‘Kurchatov Institute’’, PNPI, 188300, Gatchina, Russia.^fAlso at Istanbul Arel University, 34295 Istanbul, Turkey.^gAlso at Goethe University Frankfurt, 60323 Frankfurt am Main, Germany.^hAlso at Key Laboratory for Particle Physics, Astrophysics and Cosmology, Ministry of Education; Shanghai Key Laboratory for Particle Physics and Cosmology; Institute of Nuclear and Particle Physics, Shanghai 200240, People's Republic of China.ⁱGovernment College Women University, Sialkot—51310. Punjab, Pakistan.

surrounding the TOF. The photon energy resolution at 1 GeV is 2.5% in the barrel and 5% in the end caps. The geometric acceptance is 93% of 4π .

The response of the BESIII detector is modeled using Monte Carlo (MC) simulation software based on GEANT4 [13]. To study signal efficiencies, mass resolutions, cross-feeds among η_c decay channels, and effects due to ISR, a series of MC data samples were generated according to the signal process $e^+e^- \rightarrow \gamma\eta_c$, where the η_c subsequently decays to the twelve channels listed above. ISR effects are modeled using KKMC [14,15]. The production of $\gamma\eta_c$ and the subsequent decays of the η_c are handled by EVTGEN [16,17] using kinematics following phase space distributions. To study background processes, we generate large samples of generic $q\bar{q}$ events as well as samples corresponding to the ISR process $e^+e^- \rightarrow \gamma_{\text{ISR}}J/\psi$, where the J/ψ either decays to the same twelve modes as the η_c or decays to $\gamma\eta_c$.

We reconstruct events of the form γX_i , where the γ is referred to as the ‘‘transition photon’’ and the X_i are the twelve different combinations of hadrons corresponding to the η_c decay channels listed above. The criteria used to select events have been optimized using both MC samples and sidebands of the η_c from data.

Charged pions and kaons are reconstructed using information from the MDC. Their angle with respect to the beam direction, θ , must satisfy $|\cos\theta| < 0.93$. Except for pions originating from K_S decays, all charged tracks are further required to pass within 10 cm of the interaction point along the beam direction and within 1 cm in a plane perpendicular to the beam. Pions (except those from K_S decays) and kaons are separated using a combination of ionization energy loss in the MDC and timing information from the TOF. For each reconstructed track, particle identification probabilities P_π and P_K are calculated based on pion and kaon hypotheses, respectively. For pions, we require $P_\pi > 10^{-5}$; for kaons, we require $P_K > 10^{-5}$ and $P_K > P_\pi$.

Photons are reconstructed in the EMC by clustering energies deposited in individual crystals. Energy clusters in the barrel region ($|\cos\theta| < 0.8$) must be greater than 25 MeV and they must be greater than 50 MeV in the end cap region ($0.86 < |\cos\theta| < 0.92$). Timing from the EMC is used to suppress electronic noise and background from unrelated events. We reject candidate transition photons that can be paired with any other energy cluster in an event to form a π^0 . In the $\pi^+\pi^-\eta$ channel, the candidate transition photon is isolated from clusters formed by charged tracks by requiring their angle of separation be greater than 17.5° .

We form π^0 and η candidates using combinations of two photons with invariant mass satisfying $107 < M(\gamma\gamma) < 163 \text{ MeV}/c^2$ and $400 < M(\gamma\gamma) < 700 \text{ MeV}/c^2$, respectively. Similarly, K_S candidates are formed using two oppositely charged tracks, assumed to be pions, satisfying $471 < M(\pi^+\pi^-) < 524 \text{ MeV}/c^2$.

From these initial lists of γ , π^\pm , K^\pm , π^0 , η , and K_S , we form all possible combinations of γX_i for each i . We perform a kinematic fit for each of these combinations to the initial four-momentum of the center-of-mass system (4C) and add one constraint (1C) for the mass of every π^0 , η , and K_S candidate. We require that the resulting χ^2 per degree of freedom (dof) be less than a value optimized separately for each X_i , ranging from 3.0 to 5.2. To avoid multiple counting, we only use the combination with the best χ^2/dof . Final reconstruction efficiencies range from 4% ($\eta_c \rightarrow 2(\pi^+\pi^-\pi^0)$) to 35% ($\eta_c \rightarrow 2(\pi^+\pi^-)$).

To determine the Born cross section at each E_{CM} , we use an unbinned maximum likelihood method to simultaneously fit the recoil-mass distributions of the transition photon associated with the twelve final states γX_i . The total fit projections from three of the six E_{CM} are shown in Fig. 1(a–c). The η_c signal is described by a nonrelativistic Breit-Wigner function with mass and width fixed to their PDG values. The Breit-Wigner function is then convolved with a histogram derived from MC describing detector resolution and effects due to ISR. The Born cross section, $\sigma(e^+e^- \rightarrow \gamma\eta_c)$, is a shared free parameter that accounts for η_c decay branching fractions, reconstruction efficiencies, corrections due to ISR effects [18,19] (evaluated using the $\sigma_{Y(4260)}$ assumption), vacuum polarization [20], and integrated luminosity.

The major backgrounds are from the continuum $q\bar{q}$ process and the J/ψ ISR process, $e^+e^- \rightarrow \gamma_{\text{ISR}}J/\psi$, where the J/ψ decays to the same channels as the η_c . The

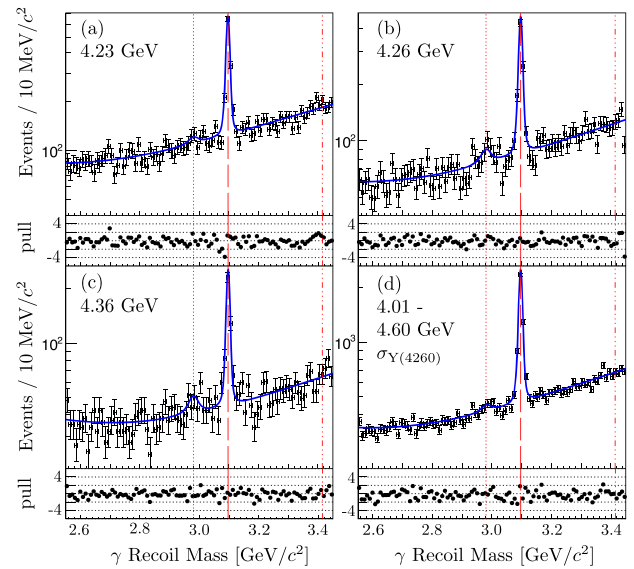


FIG. 1. The recoil-mass distribution of the transition photon summed over all η_c decay channels. Results from the simultaneous fits are overlaid. In (a–c) the fits are performed separately at each energy; in (d) the data are combined and fit with the $\sigma_{Y(4260)}$ hypothesis. Pull distributions are shown below each plot. Dotted, dashed, and dot-dashed vertical lines indicate the η_c , J/ψ , and $\chi_{c0}(1P)$ masses, respectively.

potential background where the J/ψ decays to $\gamma\eta_c$ has been found to be negligible. The continuum background is described independently in each decay channel using a second order polynomial function. The peaking J/ψ ISR background is parametrized by a double Gaussian function whose parameters are fixed using MC studies. The size of the J/ψ ISR background is allowed to float independently in each decay channel.

Since the J/ψ ISR cross section, $\sigma(e^+e^- \rightarrow \gamma_{\text{ISR}}J/\psi)$, can be accurately calculated using a combination of the ISR rate [18] and $\sigma(e^+e^- \rightarrow J/\psi)$ [21], this process serves as an important cross-check to the η_c analysis. When we perform a simultaneous fit that constrains the size of the J/ψ ISR background among the X_i using known J/ψ decay branching fractions, we obtain the results shown in Fig. 2(a). There is good agreement between the measurements and the theoretical predictions. We also obtain good agreement with the average J/ψ cross section when the size of the J/ψ ISR background is not constrained among the X_i , although with less precision.

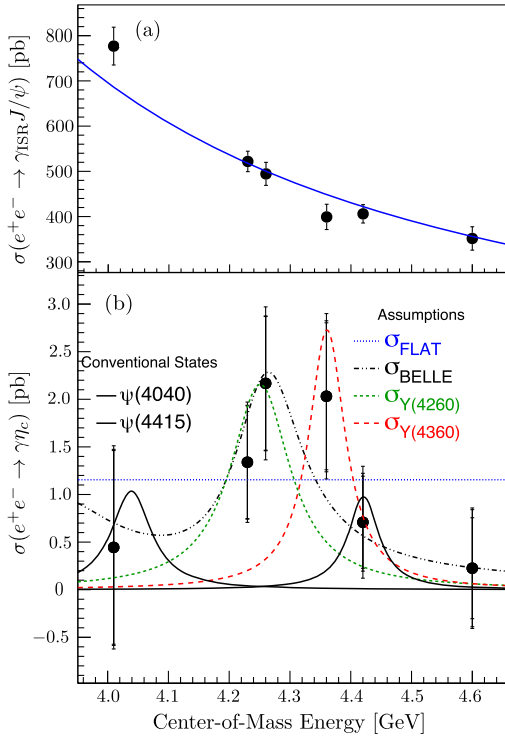


FIG. 2. (a) The cross section for $e^+e^- \rightarrow \gamma_{\text{ISR}}J/\psi$ (points) compared to the theoretical calculation (line) [18,21]. (b) The Born cross section for $e^+e^- \rightarrow \gamma\eta_c$ measured at each E_{CM} (points) and measured using the sum of all the data under various assumptions about the energy-dependence of the cross section (broken lines). The innermost tick marks are due to the statistical uncertainty, the intermediate tick marks include systematic uncertainties uncorrelated in energy (see Table III), and the outermost tick marks are the total uncertainties. The predicted cross sections for $e^+e^- \rightarrow \psi(4040) \rightarrow \gamma\eta_c$ and $e^+e^- \rightarrow \psi(4415) \rightarrow \gamma\eta_c$ [3] are shown as solid lines.

TABLE I. Measurements of the Born cross section $\sigma(e^+e^- \rightarrow \gamma\eta_c)$ (where the first uncertainty is statistical and the second is systematic), statistical significance (sig.), and 90% confidence level upper limits (U.L.) at each E_{CM} .

E_{CM} (GeV)	$\sigma(e^+e^- \rightarrow \gamma\eta_c)$ (pb)	sig. (σ)	U.L. (pb)
4.01	$0.44 \pm 1.02 \pm 0.32$	0.4	2.4
4.23	$1.34 \pm 0.59 \pm 0.22$	2.2	2.2
4.26	$2.17 \pm 0.70 \pm 0.39$	3.0	3.2
4.36	$2.03 \pm 0.77 \pm 0.40$	2.7	3.2
4.42	$0.71 \pm 0.48 \pm 0.33$	1.4	1.6
4.60	$0.23 \pm 0.53 \pm 0.35$	0.4	1.4

Our final measurements of $\sigma(e^+e^- \rightarrow \gamma\eta_c)$ are listed in Table I and are shown as the points in Fig. 2(b). These use the $\sigma_{Y(4260)}$ assumption for the calculation of effects due to ISR. The other assumptions are also used and the differences range from 1% to 6%, which are included in the systematic uncertainties. Significances of the η_c signal are obtained by comparing the likelihoods of fits with and without the η_c signal. The largest significance (3.0σ) is found at $E_{\text{CM}} = 4.26$ GeV. Upper limits of the Born cross section (at 90% confidence level) are calculated by first convolving the likelihood function with a Gaussian function whose width corresponds to the total systematic uncertainty, then integrating the resulting likelihood function up to the value that includes 90% of the integral.

We next combine all six energies under various assumptions for the energy-dependence of the cross section. In this case, we perform a simultaneous fit to the 6×12 recoil-mass distributions of the transition photon. At each energy, the $\gamma\eta_c$ cross section is constrained to be the same, as before. But between the different energies, the cross section is now constrained to follow the σ_{FLAT} , σ_{BELLE} , $\sigma_{Y(4260)}$, or $\sigma_{Y(4360)}$ cross section assumptions. Table II lists the final peak cross sections using this method, where the peak is measured at 4.26 GeV for the $\sigma_{Y(4260)}$ and σ_{BELLE} assumptions, and at 4.36 GeV for $\sigma_{Y(4360)}$. The statistical significances of the η_c signal and the upper limits on the Born cross sections are determined as before. The lines in Fig. 2(b) show the resulting cross sections as a function of energy. The statistical significance of the $\gamma\eta_c$ process is at least 3.6σ , regardless of our input cross section assumption.

TABLE II. Measurements of the peak Born cross section $\sigma_{\text{peak}}(e^+e^- \rightarrow \gamma\eta_c)$ under various assumptions for the energy-dependence of the cross section.

Assumption	$\sigma_{\text{peak}}(e^+e^- \rightarrow \gamma\eta_c)$ (pb)	sig. (σ)	U.L. (pb)
σ_{FLAT}	$1.16 \pm 0.27 \pm 0.20$	4.1	1.6
σ_{BELLE}	$2.27 \pm 0.49 \pm 0.39$	4.5	3.1
$\sigma_{Y(4260)}$	$2.11 \pm 0.49 \pm 0.36$	4.2	2.9
$\sigma_{Y(4360)}$	$2.72 \pm 0.71 \pm 0.46$	3.6	3.9

While we find evidence for $e^+e^- \rightarrow \gamma\eta_c$ in our combined fits, we are unable to distinguish between the different assumptions for the energy dependence of the cross section. To test the significance of the $\sigma_{Y(4260)}$ shape, we compare the likelihood value of a fit assuming a combination of $\sigma_{Y(4260)}$ and σ_{FLAT} (where the sizes of both components are free parameters in the fit) to that of the fit assuming σ_{FLAT} . In this test, we find the significance of the $\sigma_{Y(4260)}$ component to be only 1.5σ . With the present data sets, we also cannot rule out contributions from the $\sigma_{Y(4360)}$ hypothesis.

If we assume the energy-dependence of the cross section follows the $\psi(4040)$, $\psi(4140)$, or $\psi(4415)$ shapes individually, the significance of $e^+e^- \rightarrow \gamma\eta_c$ is 1.9σ , 3.5σ , or 1.9σ , respectively. Partial widths for $e^+e^- \rightarrow \psi(4040) \rightarrow \gamma\eta_c$ and $e^+e^- \rightarrow \psi(4415) \rightarrow \gamma\eta_c$ are calculable using the models discussed in [3]. These processes are shown as the solid lines in Fig. 2(b).

Estimates of the systematic uncertainty on the cross section measurements, discussed individually below, are summarized in Table III. The total systematic uncertainty is obtained by adding the individual systematic uncertainties in quadrature.

One of the largest systematic uncertainties comes from uncertainty in the branching fractions of the η_c decays. We estimate this uncertainty by performing many trials of our simultaneous fitting procedure using different input η_c branching fractions, which are randomly generated according to their uncertainties. When available, we use the branching fractions measured by BESIII in Ref. [22]. Since those measurements were performed by taking the ratio of $\mathcal{B}(\psi(2S) \rightarrow \pi^0 h_c(1P)) \times \mathcal{B}(h_c(1P) \rightarrow \gamma\eta_c) \times \mathcal{B}(\eta_c \rightarrow X_i)$ with $\mathcal{B}(\psi' \rightarrow \pi^0 h_c(1P)) \times \mathcal{B}(h_c(1P) \rightarrow \gamma\eta_c)$, we account for correlated errors by first randomly varying the denominator (the double product), then varying the numerator (the

triple product) for each X_i , and derive η_c branching fractions using the common denominator. The RMS of the resulting $e^+e^- \rightarrow \gamma\eta_c$ cross sections are taken as the systematic uncertainty. Note that the η_c branching fraction measurements include systematic uncertainties due to the substructure in η_c decays.

In our baseline fits to the recoil-mass distribution of the transition photon, we use a resolution derived from MC for both the η_c signal and the J/ψ ISR background. By studying the J/ψ ISR peak in its largest decay channels, we have found the resolution in data is wider than that in MC by up to 20%. We estimate the systematic uncertainty that this introduces by repeating the fits with a resolution widened by a factor of 1.2.

To estimate the uncertainty caused by fixing the η_c mass and width to their PDG averages, we vary them by $\pm 1\sigma$, repeat the fits, and take the largest difference as a systematic uncertainty. Our nominal values of the E_{CM} are taken from Ref. [8], but an uncertainty in the E_{CM} can cause a $0.75 \text{ MeV}/c^2$ shift in the apparent mass of the η_c . We also vary the input η_c mass by $\pm 0.75 \text{ MeV}/c^2$ to account for this possibility.

To account for a possible distortion in the η_c signal shape due to the photon energy-dependence of electromagnetic transitions [23,24], we repeat the fit using the η_c signal shape developed in Ref. [24].

We assign an uncertainty of 2% per charged pion and kaon to account for uncertainty in the track reconstruction efficiency (including particle ID) [25,26]. The error due to uncertainty in photon reconstruction efficiencies is 1% per photon (including photons from π^0 and η) [27]. The total error attributed to the K_S reconstruction efficiency (arising from a combination of geometric acceptance, tracking efficiency, and selection efficiency) is 4% per K_S [28]. We vary the efficiency in each η_c channel by its positive and negative extremes, refit data, and take the largest difference with respect to the nominal measurement as the systematic uncertainty.

Uncertainties in the kinematic fitting efficiencies are evaluated following the method in Ref. [29].

To judge our sensitivity to the background shape, we try a third order polynomial function in place of the second order polynomial function used in the baseline fits. We take the difference as a systematic uncertainty.

In the baseline fits, the size of the J/ψ peak is allowed to float independently in each channel. We also fix the relative size of the J/ψ peak among channels using known J/ψ branching fractions and take the difference as a systematic uncertainty.

In summary, we search for the process $e^+e^- \rightarrow \gamma\eta_c$ at six E_{CM} between 4.01 and 4.60 GeV using 4.6 fb^{-1} of data collected by BESIII. The significance is consistently above 3σ when we combine data sets according to the four assumptions listed above. We note that the cross section

TABLE III. Systematic errors (in percent) on the cross section measured at each E_{CM} and for all E_{CM} combined (All). Errors with an asterisks (*) are correlated among E_{CM} .

E_{CM} (GeV)	4.01	4.23	4.26	4.36	4.42	4.60	All
* $\mathcal{B}(\eta_c \rightarrow X_i)$	41	9	12	11	18	38	7
* Mass resolution	43	6	8	6	17	42	10
* η_c mass and width	10	1	2	3	3	3	1
e^+e^- beam energy	7	1	1	2	1	3	1
* η_c lineshape	4	7	1	5	30	31	3
* Tracking efficiency	16	7	9	9	8	12	8
* Photon efficiency	2	3	4	3	4	4	3
* K_S efficiency	2	1	2	1	1	3	4
* Kinematic fitting	5	1	1	3	2	2	2
Background Shape	29	4	2	7	23	123	5
J/ψ peak	20	4	1	1	7	62	2
σ_E assumption	2	2	3	5	3	6	
Luminosity	1	1	1	1	1	1	1
Total	73	16	18	20	47	153	17

EVIDENCE FOR $e^+e^- \rightarrow \gamma\eta_c(1S) \dots$

PHYSICAL REVIEW D **96**, 051101(R) (2017)

is better explained by $\sigma_{Y(4260)}$ than by conventional charmonium states: $\psi(4040)$, $\psi(4160)$, and $\psi(4415)$.

If we assume $e^+e^- \rightarrow \gamma\eta_c$ proceeds through a $Y(4260)$, we measure $\sigma_{\text{peak}}(e^+e^- \rightarrow \gamma\eta_c) = 2.11 \pm 0.49(\text{stat.}) \pm 0.36(\text{syst.})$ pb. Combining this with a previous BESIII measurement of $\sigma(e^+e^- \rightarrow \pi^+\pi^-J/\psi)$ [30] at 4.26 GeV, we estimate $\mathcal{B}(Y(4260) \rightarrow \gamma\eta_c)/\mathcal{B}(Y(4260) \rightarrow \pi^+\pi^-J/\psi) = 0.034 \pm 0.009$, where the statistical and systematic uncertainties have been combined.

In an alternate fit to the data shown in Fig. 1, except using only the $2(\pi^+\pi^-)$ decay channel, we include a $\chi_{c0}(1P)$ component that is also assumed to follow the $\sigma_{Y(4260)}$ hypothesis. We find $\sigma_{\text{peak}}(e^+e^- \rightarrow \gamma\chi_{c0}(1P)) < 4.6$ pb, which, after combining uncertainties, leads to the ratio $\sigma_{\text{peak}}(e^+e^- \rightarrow \gamma\chi_{c0}(1P))/\sigma_{\text{peak}}(e^+e^- \rightarrow \gamma\eta_c) < 2.8$. Although we are unable to unambiguously determine the production mechanism of $\gamma\eta_c$, the enhancement in $e^+e^- \rightarrow \gamma\eta_c$ between 4.23 and 4.36 GeV may suggest production via a hybrid charmonium state.

ACKNOWLEDGMENTS

The authors would like to thank Eric Swanson for useful discussions about conventional charmonium decays to $\gamma\eta_c$. The BESIII collaboration thanks the staff of BEPCII and the IHEP computing center for their strong support. This work is supported in part by National Key Basic Research Program of China under Contract No. 2015CB856700;

National Natural Science Foundation of China (NSFC) under Contracts Nos. 11235011, 11335008, 11425524, 11625523, 11635010; the Chinese Academy of Sciences (CAS) Large-Scale Scientific Facility Program; the CAS Center for Excellence in Particle Physics (CCEPP); Joint Large-Scale Scientific Facility Funds of the NSFC and CAS under Contracts Nos. U1332201, U1532257, U1532258; CAS under Contracts Nos. KJCX2-YW-N29, KJCX2-YW-N45, QYZDJ-SSW-SLH003; 100 Talents Program of CAS; National 1000 Talents Program of China; INPAC and Shanghai Key Laboratory for Particle Physics and Cosmology; German Research Foundation DFG under Contracts Nos. Collaborative Research Center CRC 1044, FOR 2359; Istituto Nazionale di Fisica Nucleare, Italy; Joint Large-Scale Scientific Facility Funds of the NSFC and CAS; Koninklijke Nederlandse Akademie van Wetenschappen (KNAW) under Contract No. 530-4CDP03; Ministry of Development of Turkey under Contract No. DPT2006K-120470; National Natural Science Foundation of China (NSFC); National Science and Technology fund; The Swedish Research Council; U.S. Department of Energy under Contracts Nos. DE-FG02-05ER41374, DE-SC-0010504, DE-SC-0010118, DE-SC-0012069; University of Groningen (RuG) and the Helmholtzzentrum fuer Schwerionenforschung GmbH (GSI), Darmstadt; WCU Program of National Research Foundation of Korea under Contract No. R32-2008-000-10155-0.

-
- [1] B. Aubert *et al.* (BABAR Collaboration), *Phys. Rev. Lett.* **95**, 142001 (2005).
- [2] C. Patrignani *et al.* (Particle Data Group), *Chin. Phys. C* **40**, 100001 (2016).
- [3] T. Barnes, S. Godfrey, and E. S. Swanson, *Phys. Rev. D* **72**, 054026 (2005).
- [4] S.-L. Zhu, *Phys. Lett. B* **625**, 212 (2005).
- [5] F. E. Close and P. R. Page, *Phys. Lett. B* **628**, 215 (2005).
- [6] J. J. Dudek, R. G. Edwards, and C. E. Thomas, *Phys. Rev. D* **79**, 094504 (2009).
- [7] M. Ablikim *et al.* (BESIII Collaboration), *Chin. Phys. C* **39**, 093001 (2015).
- [8] M. Ablikim *et al.* (BESIII Collaboration), *Chin. Phys. C* **40**, 063001 (2016).
- [9] G.-Z. Xu, Y.-J. Li, K.-Y. Liu, and Y.-J. Zhang, *J. High Energy Phys.* **10** (2014) 71.
- [10] Z. Q. Liu *et al.* (Belle Collaboration), *Phys. Rev. Lett.* **110**, 252002 (2013).
- [11] D. M. Asner *et al.*, *Int. J. Mod. Phys. A* **24**, 499 (2009).
- [12] M. Ablikim *et al.* (BESIII Collaboration), *Nucl. Instrum. Methods Phys. Res., Sect. A* **614**, 345 (2010).
- [13] S. Agostinelli *et al.* (GEANT4 Collaboration), *Nucl. Instrum. Methods Phys. Res., Sect. A* **506**, 250 (2003).
- [14] S. Jadach, B. F. L. Ward, and Z. Was, *Comput. Phys. Commun.* **130**, 260 (2000).
- [15] S. Jadach, B. F. L. Ward, and Z. Was, *Phys. Rev. D* **63**, 113009 (2001).
- [16] D. J. Lange, *Nucl. Instrum. Methods Phys. Res., Sect. A* **462**, 152 (2001).
- [17] P. Rong-Gang, *Chin. Phys. C* **32**, 599 (2008).
- [18] V. P. Druzhinin, S. I. Eidelman, S. I. Serebnyakov, and E. P. Solodov, *Rev. Mod. Phys.* **83**, 1545 (2011).
- [19] E. A. Kuraev and V. S. Fadin, *Sov. J. Nucl. Phys.* **41**, 466 (1985).
- [20] S. Actis *et al.* (Working Group on Radiative Corrections and Monte Carlo Generators for Low Energies), *Eur. Phys. J. C* **66**, 585 (2010).
- [21] G. S. Adams (CLEO Collaboration), *Phys. Rev. D* **73**, 051103 (2006).
- [22] M. Ablikim *et al.* (BESIII Collaboration), *Phys. Rev. D* **86**, 092009 (2012).

M. ABLIKIM *et al.*

PHYSICAL REVIEW D **96**, 051101(R) (2017)

- [23] R. E. Mitchell (CLEO Collaboration), *Phys. Rev. Lett.* **102**, 011801 (2009); **106**, 159903(E) (2011).
- [24] V. V. Anashin *et al.*, *Int. J. Mod. Phys. Conf. Ser.* **02**, 188 (2011).
- [25] M. Ablikim *et al.* (BESII Collaboration), *Phys. Rev. Lett.* **107**, 092001 (2011).
- [26] M. Ablikim *et al.* (BESIII Collaboration), *Phys. Rev. D* **83**, 112005 (2011).
- [27] M. Ablikim *et al.* (BESIII Collaboration), *Phys. Rev. D* **92**, 052003 (2015); **93**, 039906(E) (2016).
- [28] M. Ablikim *et al.* (BESIII Collaboration), *Phys. Rev. D* **87**, 052005 (2013).
- [29] M. Ablikim *et al.* (BESIII Collaboration), *Phys. Rev. Lett.* **111**, 242001 (2013).
- [30] M. Ablikim *et al.* (BESIII Collaboration), *Phys. Rev. Lett.* **110**, 252001 (2013).